Attentional ShapeContextNet for Point Cloud Recognition

Saining Xie* Sainan Liu* Zeyu Chen Zhuowen Tu
University of California, San Diego
{s9xie, sal131, zec003, ztu}@ucsd.edu

Abstract

We tackle the problem of point cloud recognition. Unlike previous approaches where a point cloud is either converted into a volume/image or represented independently in a permutation-invariant set, we develop a new representation by adopting the concept of shape context as the building block in our network design. The resulting model, called ShapeContextNet, consists of a hierarchy with modules not relying on a fixed grid while still enjoying properties similar to those in convolutional neural networks — being able to capture and propagate the object part information. In addition, we find inspiration from self-attention based models to include a simple yet effective contextual modeling mechanism — making the contextual region selection, the feature aggregation, and the feature transformation process fully automatic. ShapeContextNet is an end-to-end model that can be applied to the general point cloud classification and segmentation problems. We observe competitive results on a number of benchmark datasets.

1. Introduction

Convolutional neural networks (CNN) [20, 19, 29, 31, 14] and their recent improvements [32, 16, 39, 43] have greatly advanced the state-of-the-arts for a wide range of applications in computer vision. Areas like classification, detection [11, 26], and segmentation [22, 13] for 2D images have witnessed the greatest advancement. Extending 2D-based convolution to 3D-based convolution for 3D computer vision applications such as 3D medical imaging [23, 10], though still effective, is arguably less explosive than the 2D cases. This observation becomes more evident when applying 3D convolution to videos [33, 4, 34, 40] where 2D frames are stacked together to form a 3D matrix. Innate priors induced from careful study and understanding of the task at hand are often necessary.

The development of large datasets of 2D static images like ImageNet [9] is one of the key factors in the recent development of deep learning technologies. Similarly, the emergence of 3D shape based datasets such as ShapeNet [5] has attracted a great deal of attention and stimulated advancement in 3D shape classification and recognition. In areas outside of computer vision, the 3D shape classification and recognition problem has been extensively studied in computer graphics [7, 12, 28] and robotics [27, 36]. Unlike 2D images where pixels are well-positioned in a strict grid framework, shapes encoded by 3D point clouds [38, 42] consist of individual points that are scattered in the 3D space where neither is there a strict grid structure nor is there an intensity value associated with each point.

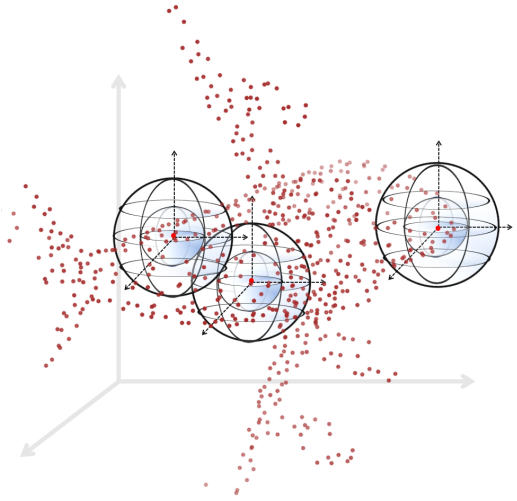

Figure 1. A motivating example to illustrate how the basic building block of our proposed algorithm, the shape context kernel, is applied to a 3D point cloud to capture the contexual shape information.

To combat the 3D point cloud classification problem, there have been previous works [17, 42, 30, 38] in which scattered 3D points are assigned to individual cells in a well structured 3D grid framework. This type of conversion from 3D points to 3D volumetric data can facilitate the extension from 2D CNN to 3D CNN but it also loses the intrinsic geometric property of the point cloud. A pioneering work, PointNet [6], addresses the fundamental representation problem for the point cloud by obtaining the in-

*Equal contributions.

trinsic invariance of the point ordering. Well-guided procedures are undertaken to capture the invariance within point permutations for learning an effective PointNet [6], achieving state-of-the-art results with many desirable properties. One potential problem with PointNet, however, is that the concept of parts and receptive fields is not explicitly addressed, because the point features in PointNet are treated independently before the final aggregation (pooling) layer. An improved work, PointNet++ [25], has recently been developed to incorporate the global shape information using special modules such as farthest point sampling and geometric grouping. Our paper instead focuses on developing a deep learning architecture for point cloud classification that connects the classic idea of *shape context* [3] to the learning and computational power of hierarchical deep neural networks [20]. We name our algorithm *ShapeContextNet* (SCN) and a motivating example is shown in Figure 1.

Before the deep learning era [19], carefully designed features like shape context [3] and inner distances [21] were successfully applied to the problem of shape matching and recognition. In *shape context*, an object is composed of a number of scattered points and there is a well-designed disc with unevenly divided cells to account for the number of neighborhood points falling into each cell; the overall features based on the occurrences of the points within every individual cells give rise to a rich representation for the object parts and shapes. *Shape context* was widely used before but kept relatively distant to the deep learning techniques.

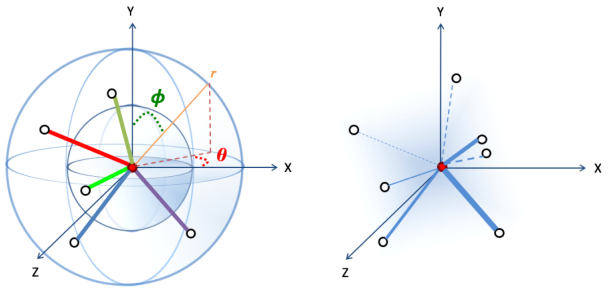

(a) (b)

Figure 2. An illustration of our shape context kernel displayed in a spherical coordinate system. (a) the shape context kernel, the number of bins on polar angle (ϕ), number of bins on azimuthal angle (θ) and number of bins on radial distance (r) are manually specified. Different colors of edges represent different binary affinity matrices indicating different bins. (b) the attentional shape context "kernel", where there is no predefined bins, and the soft affinity matrix, or attention weights (indicated by edge thickness) are learned during training.

Motivated by the rich representational power of *shape context* [3], as well as the recent success in deep convolutional neural networks [19], we propose a new method, ShapeContextNet (SCN) that adopts *shape context* as the basic building block acting like convolution in CNN. The basic network architecture of SCN is illustrated in Figure 4 with the basic shape context descriptor shown in Figure 2. We do not force a given set of points into volumetric data, nor do we remove the spatial relationship of the points. Instead, we build layers of shape context to account for the local and the global contextual information in a hierarchy learned by an end-to-end procedure. In order to incorporate the local shape context descriptor into a neural network, we break a *shape context block* into three key components, namely *selection*, *aggregation*, and *transformation*. For a point p_i in the point cloud $\{p_1, p_2, \ldots, p_i, \ldots, p_N\}$, the set of all $N-1$ points forms a rich context depicting the shape information centered at p_i. However, using all the neighborhood points might be computational and spatially unattractive. We instead design *shape context kernel* with distributed bins in the log-polar space, shown in Figure 2 which is inspired by the *shape context* descriptor [3]. The *selection* operation thus decides a set of neighboring points of p_i to define coarse groups of neighboring points for p_i to attend to. The *aggregation* operation (such as histogram, or pooling) builds a robust descriptor that captures the distribution over relative positions. The *transformation* operation projects the descriptor to a high-dimensional feature space by fusing features from different neighboring points or groups. Like in the standard CNN, SCN propagates the local part information through hierarchical layers to capture the rich local and global shape information.

Although the concept of building deep *shape context* is simple, we still face many implementation choices in practice: how to design the *shape context* bins and handle the additional computation cost for computing "point to bin" relationships, how to choose an aggregation operation that preserves feature discriminability, etc. We are inspired by the recent development in attention-based models that are mainly applied in natural language processing tasks such as sequence-to-sequence modeling [2, 41]. A self-attention approach is proposed in [35] and achieves state-of-the-art results on the neural machine translation task with an architecture design that consists of a stack of self-attention blocks. The dot-product self-attention block has no recurrence — keys, values and queries come from the same place and is highly efficient in computation. We connect the self-attention idea with *shape context* within a supervised learning setting. Self-attention combines the selection and aggregation process into a single soft alignment operation. The resulting model enjoys the property of *shape context* and is an end-to-end trainable architecture without the bells and whistles of a handcrafted selection operation (bins). We call it *Attentional ShapeContextNet* (A-SCN).

We apply SCN and A-SCN to 3D point shape classification and segmentation datasets [38, 42] and observe improved results over the PointNet [6] model.

2. Method

2.1. Revisiting the *Shape Context* Descriptor

We first briefly describe the classic *shape context* descriptor, which was introduced in a seminal work [3] for 2D shape matching and recognition. One main contribution in [3] is the design of the shape context descriptor with spatially inhomogeneous cells. The neighborhood information for every point in a set is captured by counting the number of neighboring points falling inside each cell. The shape descriptor for each point is thus a feature vector (histogram) of the same dimension as the number of the cells with each feature dimension depicting the number of points (normalized) within each cell. The shape context descriptor encodes the rich contextual shape information using a high-dimensional vector (histogram) which is particularly suited for matching and recognition objects in the form of scattered points. For each point p_i in a give point set, *shape context* computes a coarse histogram h_i of the relative coordinates of the neighboring point,

$$h_i(l) = \#\{p_j \neq p_i : (p_j - p_i) \in bin(l)\}.$$

Shape context uses a log-polar coordinate system to design the bins. Figure 3 shows a basic 2D shape context descriptor used in our method (note that we make the center cells larger which is slightly different to the original shape context [3] design where the center cells are relatively small).

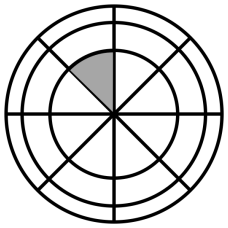

Figure 3. Example of a 2D shape context kernel with 24 bins ($n_r = 3$ and $n_\theta = 8$).

There were also attempts to extend *shape context* to 3D. In [18] concentric shells, polar angle ϕ and azimuthal angle θ are considered to divide the space into different quadrants. We use a similar design for our bins, as is shown in Figure 2 (a). Although shape context is considered as one of the most successful descriptors in computer vision, its integration into the modern deep learning framework has been under-explored.

2.2. A General Formulation

In this section, we introduce a generalized formulation for *shape context* to build our deep ShapeContextNet. Let a given point set (cloud) for one shape be $P = \{p_1, p_2, \cdots, p_i, \cdots, p_N\}$. Each $p_i \in \mathcal{R}^3$ is a point represented by its 3D coordinates. Our proposed ShapeContextNet (SCN) is a neural network architecture (shown in Figure 4) with its basic building block being SCN block (illustrated in Figure 2 (a)). Each SCN block consists of three operations: *selection*, *aggregation*, and *transformation*, which will be explained in detail below.

Selection. For a point cloud P of N points, the selection operation is to produce an affinity matrix $A \in \{0,1\}^{N\times N}$, where $A(i,j) = 1$ indicates that a point p_j has an edge to a reference point p_i, while $A(i,j) = 0$ indicates that a point p_j has no connection to point p_i. The connected component centered at point p_i is a representation of the global shape arrangement. In the original *shape context*, the selection operation first divides the space into L bins. In that case, instead of having a single affinity matrix, we build L disjoint affinity matrices simultaneously, and $A^l(i,j) = 1$ means $p_j \in bin(l)$ of the reference point p_i, for $l = 1, \cdots, L$. Note that the selection operations do not necessarily rely on any predefined partitioning of space, and can be automatically learned in the same vein as attention mechanism, where the A is the $N \times N$ attention weight. The attentional selection operation can either be hard or soft assignments.

Aggregation. After the selection operations, to form a compact representation of shape arrangement at a reference point p_i, we need to aggregate the information from the selected points. We denote an aggregation function as m. In original *shape context*, for N points and L bins, and a reference point p_i, we have L aggregation functions $m_i^l, l = 1, \cdots, L$, which together form the histogram representation. Each m_i^l is a counting function that counts the number of points in $bin(l)$, which can be represented as a sum pooling function $m_i^l = \sum_j \mathbb{1}[A^l(i,j) = 1]$.

In a more general form, m can be a weighted sum operator (dot product) such that $m_i = \sum_j A(i,j) \cdot \hat{p}_j$ using the learned attention weights A. $\hat{p}_j$ could be simply the input coordinates p_j, or any arbitrary feature vector associated with that point.

Transformation. Now we have an aggregated representation for the reference point p_i. It is natural to add a feature transformation function f to incorporate additional non-linearity and increase the capacity of the model. In the original *shape context*, after a local descriptor is built, a discriminative classifier, e.g. a support vector machine, can be added for the final classification task. The transformation can be realized by a kernel function such as a radial basis function. In the context of deep neural networks, an MLP, or convolutional layer with a non-linear activation function can be used for the feature transformation purpose.

Shape context block. After we introduce the above three operations, the *shape context* descriptor SC can be formulated as,

$$SC_i = f(h_i) = f([h_i(1), \cdots, h_i(L)]) = f([m_i^1, \cdots, m_i^L])$$

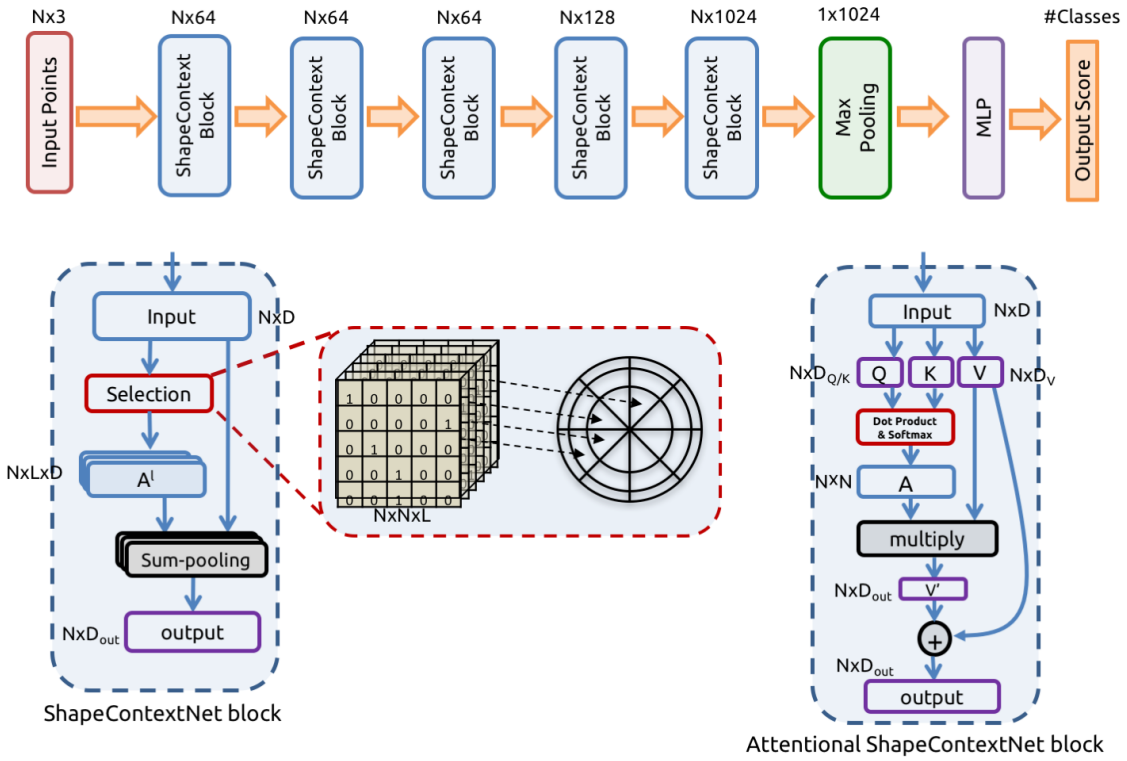

Figure 4. **ShapeContextNet (SCN) and Attentional ShapeContextNet (A-SCN) architectures.** The classification network has 5 ShapeContext blocks; each block takes N point feature vectors as input, and applies the selection, aggregation and transformation operations sequentially. The ShapeContext blocks can be implemented by hand-designed shape context kernels (SCN block), or a self-attention mechanism learned from data (A-SCN block). See text in Section 2 for details.

where $m_i^l = \sum_j \mathbb{1}[A^l(i,j) = 1]$. Note that every components in this formulation can be implemented by a back-propagatable neural network module, and thus, similar to a convolutional layer, SC is a compositional block that can be used to build a shape context network,

$$SCNet = SC_i(SC_i(SC_i(\cdots)))$$

2.3. ShapeContextNet

Shape context kernel. Similar to [18], we use concentric shells to design the shape context kernel. The kernel is adjustable with three parameters: polar angle ϕ, azimuthal angle θ and radial distance r (Figure 2 (a)). In our setting, ϕ and θ are evenly divided into different sectors, while for r, a logarithmic parametrization of the shell radii is used. We also set a maximum radius of the sphere max R, which defines the receptive field size for a single shape context kernel. Thus the design of the shape context kernel is paramerized by the maximum radius (max R), the number of bins for radius r (n_r), angles θ (n_θ) and angles ϕ (n_ϕ). The combined number of bins for a shape context kernel is equal to $n_r \times n_\theta \times n_\phi$.

Selection. With the L bins induced by a shape context kernel, the selection operation builds L disjoint affinity matrices $A^1, \cdots, A^L$, where each matrix is corresponding to a specific bin. We generate the affinity matrices online during training and share them across different layers.

Aggregation. Following original *shape context*, the aggregation operation is simply a sum-pooling layer that aggregates points (associated with D-dimensional feature vectors) within each bin. Note that the sum-pooling layer can be implemented by L parallel matrix multiplications, as A^L is binary. The aggregation operation results in L sets of pooled features, thus the output is a tensor of shape $N \times L \times D$.

Transformation. Finally the transformation operation is realized by a convolutional layer with a $[L, 1]$ kernel that fuses L sets of feature points and projects them to (higher dimensional) output feature vectors of D_{out}. A ShapeContext block consists of above operations and our ShapeContextNet is a stack of ShapeContext blocks with increasing output dimensions of D_{out}. We follow the overall network configuration of PointNet and use $D_{out} = (64, 64, 64, 128, 1024)$ as the output dimensions for each ShapeContext block.

Limitations. While being conceptually simple and en-

joying good properties of classic *shape context* descriptors such as translation-invariance, handcrafting shape context kernels are not straight-forward and hard to generalize across different point cloud datasets which usually have varying size and density. This motivates us to propose the following attention-based model.

2.4. Attentional ShapeContextNet

We now introduce a different approach inspired by research in natural language processing (sequence-to-sequence) tasks. Traditional sequence-to-sequence models usually adopt recurrent neural networks (e.g. LSTM[15]), external memory or temporal convolutions to capture the context information. The dot-product self-attention proposed in [35] is a model that handles long path-length contextual modeling by a light-weight gating mechanism, where the attention weight matrix is generated using a simple dot-product. It is worth-noting that self-attention is also invariant to the input ordering. Unlike traditional attention-based sequence-to-sequence models, in a self-attention block, *query* vector $Q \in \mathcal{R}^{D_Q}$, *key* vector $K \in \mathcal{R}^{D_K}$ (usually $D_Q = D_K$) and *value* vector $V \in \mathcal{R}^{D_V}$ are learned from the same input. In a supervised classification setting, one can think Q, K and V are just three feature vectors learned by three independent MLP layers. Attention weights are computed by a dot product of Q and K, and then multiplied with V to obtain the transformed representation.

Figure 2 shows the similarities and differences between manually specified shape context kernels and the automatically learnable self-attention mechanism: They all aim to capture the distribution over relative positions; they are unified under the same formulation in Section 2.2; the selection operation in self-attention does not rely on hand-designed bin partitioning as it can be learned from data; self-attention has better modeling capability by adopting a weighted sum aggregation function, in contrast to using a simple sum-pooling function.

Selection and Aggregation. We consider computing self-attention on the whole point cloud P of size N. The selection operation produces a soft affinity matrix, which is the self-attention weight matrix A of size $N \times N$, the aggregation operation is transforming the value vector V with weight matrix A by a dot product,

$$\text{Attention}(Q, V, K) = \text{Softmax}(\frac{QK^T}{\sqrt{D_Q}}) \cdot V \qquad (1)$$

Transformation. MLPs with ReLU activation function can be added as a feature transformation operation after each self-attention operation (Equation 1). To further improve the model expressiveness, we add a simple feature gating layer to the MLP, similar to [8, 24].

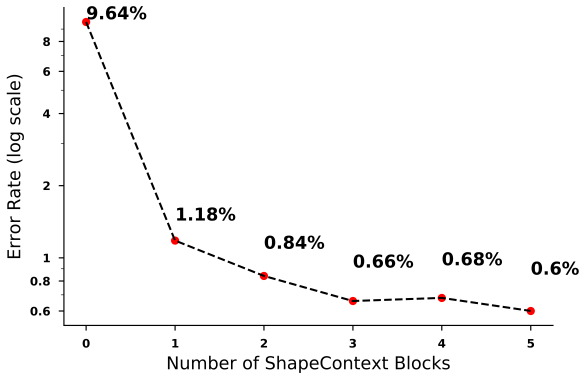

Figure 5. **Ablation analysis on the number of ShapeContext blocks.** The error rates obtained by increasing the number of ShapeContext blocks. Metric is overall accuracy on 2D MNIST test set (N = 256). The bin configuration is: max $R = 0.5$, $n_r = 3$, $n_\theta = 12$.

Model	N	Error rate (%)
PointNet[6]	256	0.78
PointNet++[25]	512	0.51
shape context local	256	1.18
ShapeContextNet	256	0.60

Table 1. 2D point cloud classification results on the MNIST dataset. ShapeContextNet achieves better performance than PointNet showing the effectiveness of contextual information; the *shape context* local model consists of only one shape context block.

3. Experimental Results

3.1. ShapeContextNets: 2D case

We first showcase the effectiveness of deep ShapeContextNet which has a stack of shape context blocks.

2D point set is generated for MNIST dataset following the same protocol as used in PointNet[6], where 256 points are sampled for each digit. We use a shape context kernel with max $R = 0.5$, $n_r = 3$ and $n_\theta = 12$, thus 36 bins in total.

Table 1 shows that a simple 5-layer SCN achieves better performance than PointNet, showing that using the distribution over relative positions as a context feature is indeed helpful for the shape recognition task. The performance of SCN is also competitive to the recent PointNet++[25] model which uses 512 points as input. *shape context* local is a model that consists of only one shape context block, which resembles the "feature extraction and classifier learning" pipeline in traditional computer vision. To better understand the importance of hierarchical learning in ShapeContextNet, in Figure 5, we vary the number of shape context blocks from 0 to 5 in the network (Figure 4), where the 5-layer model is our ShapeContextNet, the 1-layer model is the *shape context* local model, and 0 means no shape con-

text block. We observe that as the number of shape context blocks increases, the error rate decreases.

3.2. ShapeContextNets: 3D case

We evaluate the 3D shape classification performance of SCN on the ModelNet40[38] dataset, with point cloud data from 12,311 CAD models in 40 categories. We use 9,843 for training and 2,468 for testing. Following [6], 1,024 points are sampled for each training/testing instance. Table 2 summarizes the impact of different shape context kernel design choices parametrized by max R, n_r, n_θ and n_ϕ.

	max R	No. of r bins	No. of θ bins	No. of ϕ bins	accuracy avg. class	accuracy overall
PointNet vanilla[6]	-	-	-	-	-	87.1
PointNet[6]	-	-	-	-	86.2	89.2
PointNet++[25]	-	-	-	-	-	**90.7**
(A)	0.25	3	3	3	86.2	89.3
(B)	1				84.8	88.6
(C)	0.5	2			86.7	89.6
(D)		4			86.5	89.6
(E)		3	2		81.4	84.8
(F)			4		82.2	84.2
(G)			3	2	85.5	88.9
(H)				4	87.5	89.7
SCN (I)	0.5	3	3	3	**87.6**	**90.0**

Table 2. **Ablation analysis on shape context kernel design in ShapeContextNet.** We evaluate SCN models with different kernel configurations (model (A)-(I)). max R is the maximum local radius for the sphere shape context kernel at each reference point. n_r, n_θ and n_ϕ are the number of different shell and angle bins. Unlisted values are identical to those of the preceding model. We report averaged and overall accuracy on ModelNet40 test set (N=1024).

We obtain the best results with max $R = 0.5$. Note that the coordinates of point cloud in ModelNet40 are normalized to $[-1, 1]$. This means the receptive field of a single shape context kernel covers around a quarter of the entire point cloud. With the same radius bin configuration, the test accuracy peaks when $n_r = n_\theta = n_\phi = 3$. Empirically, the number of r bins has the least impact on the test accuracy, whereas the number of θ bins appears to be crucial for the performance. With minimal change in architecture to a *vanilla* PointNet (by replacing the MLP layers to carefully designed shape context kernels), ShapeContextNet (model (I)) achieves better or competitive results compared to full PointNet model (with additional input/feature transformation layers), and the recent PointNet++ model (with special sampling/grouping modules).

3.3. Attentional ShapeContextNet

ModelNet40 Shape Classification. The architecture of Attentional ShapeContextNet (A-SCN) follows the general design of ShapeContextNet (SCN). In contrast to using hand-crafted shape context kernels, we adopt the self-attention module as the shape context block in the network (Figure 4). Q, K and V feature vectors are learned from the input using three MLPs. We use $D_K = D_Q = (32, 32, 32, 32, 64)$ and $D_V = D_{out} = (64, 64, 64, 128, 1024)$ for each block. Attention weight matrix of shape $N \times N$ is computed according to Equation 1. Table 3 summarizes the performance of A-SCN with different hyperparameters. The choices of different hyperparameters are generally aligned with those in [35] on the machine translation task. For example, the residual connection is necessary in order to learn a good model, and learning Q and K vectors independently is better than weight-sharing. Note that similar to SCN where L affinity matrices are used, we can also learn multiple attention weights in parallel for A-SCN. This is called *multi-head attention* in [35]. However, empirically we find that using multi-head attention does not yield better performance comparing to the one-head model, and introduces additional computation overhead. Therefore, in this paper A-SCN refers to our one-head model (model (E)). A-SCN is able to achieve 89.8% overall accuracy, which is on par with SCN, but with a simpler design and fewer critical hyper-parameter to set.

A-SCN	Q=K?	ReLU Q/K/V	BN Q/K/V	residual connect.	Num of heads	accuracy avg. class	accuracy overall
(A)	✓	✓/✓/✓	✓/✓/✓	✓	1	85.7	89.0
(B)				✗		28.2	36.7
(C)	✗			✓		85.7	89.1
(D)		✗/✗/✗				86.1	89.2
(E)			✗/✗/✓			**87.4**	**89.8**
(F)					2	86.3	89.2
(G)					4	87.2	89.8

Table 3. **Ablation analysis on the Attentional ShapeContextNet architecture.** We evaluate the Attentional ShapeContextNet model on ModelNet40 dataset with different hyperparameter settings (model (A)-(G)). We report class-averaged and overall accuracy on test set. Unlisted values are identical to those of the preceding model. Q, K and V here represent the feature vectors learned in an A-SCN block (Figure 4).

In Figure 6 we show surprisingly diverse and semantically meaningful behavior of the learned attention weights. For a reference point, it oftentimes attends to areas far away to itself. The selected areas are usually descriptive and discriminative parts of a model, e.g. back or legs of a chair. Figure 7 visualizes how shape information is propagated and condensed into a compact representation in a multi-level neural network. For a fixed reference points, attention becomes increasingly sparse, and focuses on smaller areas when the level gets higher.

ShapeNet Part Segmentation. Part segmentation is a challenging task in 3D object recognition domain. Given a set of points of a 3D shape model (e.g. a plane), the part segmentation task is to label each point in the set as one of the model's part (e.g. engine, body, wing and tail). We follow the experimental setup in [6], and defines the task as a point-wise classification problem.

Our model (A-SCN) is trained and evaluated on

	mean	aero	bag	cap	car	chair	ear phone	guitar	knife	lamp	laptop	motor	mug	pistol	rocket	skate board	table
# shapes		2690	76	55	898	3758	69	787	392	1547	451	202	184	283	66	152	5271
Wu [37]	-	63.2	-	-	-	73.5	-	-	-	74.4	-	-	-	-	-	-	74.8
Yi [42]	81.4	81.0	78.4	77.7	75.7	87.6	61.9	**92.0**	85.4	82.5	95.7	**70.6**	91.9	**85.9**	53.1	69.8	75.3
3DCNN[6]	79.4	75.1	72.8	73.3	70.0	87.2	63.5	88.4	79.6	74.4	93.9	58.7	91.8	76.4	51.2	65.3	77.1
PointNet++[25]	**85.1**	82.4	79.0	**87.7**	77.3	**90.8**	71.8	91.0	85.9	**83.7**	95.3	**71.6**	**94.1**	81.3	58.7	**76.4**	**82.6**
PointNet[6]	83.7	83.4	78.7	82.5	74.9	89.6	**73.0**	91.5	85.9	80.8	95.3	65.2	93.0	81.2	57.9	72.8	80.6
A-SCN (ours)	84.6	**83.8**	**80.8**	83.5	**79.3**	90.5	69.8	**91.7**	**86.5**	82.9	**96.0**	69.2	93.8	82.5	**62.9**	74.4	80.8

Table 4. **Segmentation results on ShapeNet part dataset.** We compared the results with Wu [37], Yi [42], 3DCNN from [6], PointNet [6] and recent PointNet++[25] which uses additional normal direction features. The results are evaluated with mean IoUs(%) metric on points. Our A-SCN model achieves competitive performance for point cloud part segmentation.

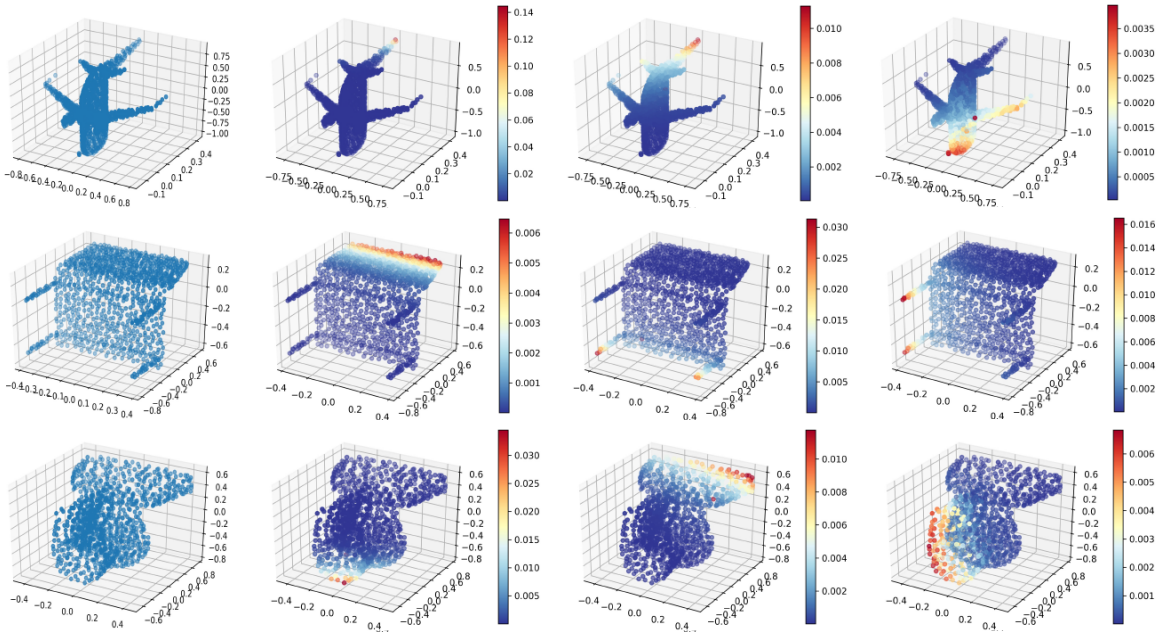

Figure 6. **Attention weights learned by A-SCN on three shape models: a plane, a chair and a toilet.** First column in each row shows the original point cloud. The other columns visualize learned weights for one randomly sampled reference point. Higher value indicates stronger connection to the reference point. Attention weights learned by A-SCN are diverse, sparse, and semantically meaningful and a reference point learns to attend to discriminative parts of a model.

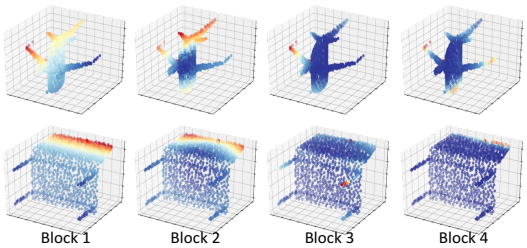

Figure 7. **Attention weights learned on different levels.** In A-SCN, shape information is propagated and condensed into a compact representation through a multi-level network structure. From left to right are attention weights, for a fixed reference point, learned in the first, second, third and fourth attentional shape context block. Attention becomes increasingly sparse, and focuses on smaller areas with compact representations.

ShapeNet part dataset following the data split from [5]. ShapeNet part dataset [42] consists of 16,881 object from 16 object categories, where each object category is labeled with 2-5 parts. During training, we randomly sample 1024 points from the 3D point cloud of each object and use cross-entropy as our loss function. We also followed the settings from [42], which assume the object category labels are known and encoded by one-hot encoding. During testing, we test the model on all the points from each object and evaluated using point mean intersection over union (mIoU), which averages IoU across all part classes similar to [6]. Our A-SCN model outperforms PointNet over most categories, and is on par with the recent PointNet++ model which augment the input points with additional normal information. Full results for part segmentation are listed in Table 4.

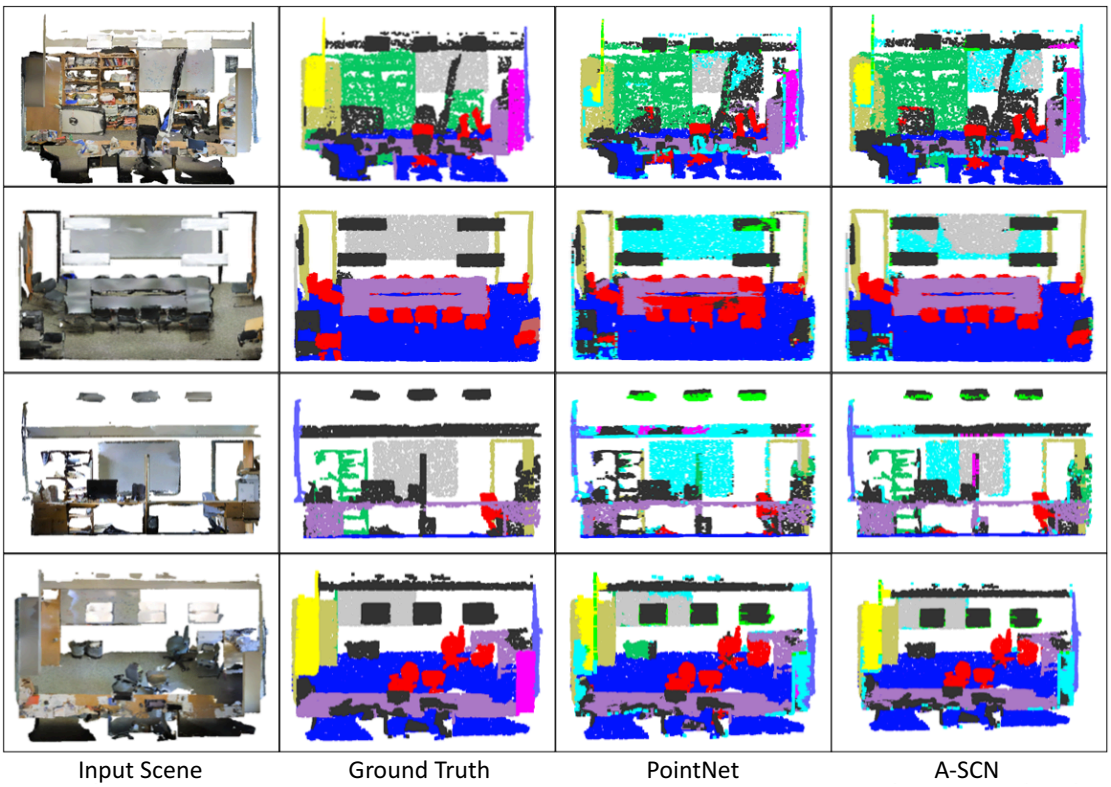

Figure 8. **Visualization of semantic segmentation results by A-SCN.** From left to right: original input scenes; ground truth point cloud segmentation; PointNet[6] segmentation results and Attentional ShapeContextNet (A-SCN) segmentation results. Color mappings are red: chairs, purple: tables , orange: sofa, gray: board, green: bookcase, blue: floors, violet: windows, yellow: beam, magenta: column, khaki: doors and black: clutters.

S3DIS Semantic Segmentation. Stanford 3D indoor scene dataset[1] includes 6 large scale areas that in total have 271 indoor scenes. Each point in the scene point cloud is associated with one label in 13 categories. We follow [6] for data pre-processing, dividing the scene point cloud into small blocks. We also use the same k-fold strategy for training and testing. We randomly sample 2,048 points from each block for training and use all the points for testing. For each point, we use the XYZ coordinates, RGB value and the normalized coordinates as its input vector.

	mean IoU(%)	overall accuracy (%)
PointNet [6]	47.71	78.62
A-SCN (ours)	**52.72**	**81.59**

Table 5. **Results on scene semantic segmentation.** Mean IoU(%) on and point-wise accuracy are reported. Our Attentional ShapeContextNet model outperforms PointNet in both metrics.

The evaluation results of our method are in Figure 5. By taking into account the global shape context in a hierarchical learning way, our A-SCN model achieves 52.72% in mean IoU and 81.59% in point-wise accuracy, improving the results by PointNet in both metrics. Some of our segmentation results are visualized in Figure 8.

4. Conclusion

To tackle the recognition problem for 3D/2D point clouds, we develop a new neural network based algorithm by adopting the concept of shape context to build our basic building block, shape context kernel. The resulting model, named as ShapeContextNet (SCN), consists of hierarchical modules that are able to represent the intrinsic property of object points by capturing and propagating both the local part and the global shape information. In addition, we propose an Attentional ShapeContextNet (A-SCN) model to automate the process for contextual region selection, feature aggregation, and feature transformation. We validated the effectiveness of our model on a number of benchmark datasets and observed encouraging results.

Acknowledgment

This work is funded by NSF IIS-1618477 and NSF IIS-1717431. S. Xie is supported by Google. The authors would like to thank Justin Lazarow for insightful discussions, Hao Su and Charles R. Qi for helping with the MNIST experiment setup.

References

[1] I. Armeni, O. Sener, A. R. Zamir, H. Jiang, I. Brilakis, M. Fischer, and S. Savarese. 3d semantic parsing of large-scale indoor spaces. In *CVPR*, 2016. 8

[2] D. Bahdanau, K. Cho, and Y. Bengio. Neural machine translation by jointly learning to align and translate. In *ICLR*, 2015. 2

[3] S. Belongie, J. Malik, and J. Puzicha. Shape matching and object recognition using shape contexts. *TPAMI*, 24(4):509–522, 2002. 2, 3

[4] J. Carreira and A. Zisserman. Quo vadis, action recognition? a new model and the kinetics dataset. In *CVPR*, 2017. 1

[5] A. X. Chang, T. Funkhouser, L. Guibas, P. Hanrahan, Q. Huang, Z. Li, S. Savarese, M. Savva, S. Song, H. Su, et al. Shapenet: An information-rich 3d model repository. *arXiv preprint arXiv:1512.03012*, 2015. 1, 7

[6] R. Q. Charles, H. Su, M. Kaichun, and L. J. Guibas. Pointnet: Deep learning on point sets for 3d classification and segmentation. In *CVPR*, 2017. 1, 2, 5, 6, 7, 8

[7] D.-Y. Chen, X.-P. Tian, Y.-T. Shen, and M. Ouhyoung. On visual similarity based 3d model retrieval. In *Computer graphics forum*, 2003. 1

[8] Y. N. Dauphin, A. Fan, M. Auli, and D. Grangier. Language modeling with gated convolutional networks. In *ICML*, 2017. 5

[9] J. Deng, W. Dong, R. Socher, L.-J. Li, K. Li, and L. Fei-Fei. ImageNet: A Large-Scale Hierarchical Image Database. In *CVPR*, 2009. 1

[10] Q. Dou, L. Yu, H. Chen, Y. Jin, X. Yang, J. Qin, and P.-A. Heng. 3d deeply supervised network for automated segmentation of volumetric medical images. *Medical Image Analysis*, 2017. 1

[11] R. Girshick, J. Donahue, T. Darrell, and J. Malik. Rich Feature Hierarchies for Accurate Object Detection and Semantic Segmentation. In *CVPR*, 2014. 1

[12] K. Guo, D. Zou, and X. Chen. 3d mesh labeling via deep convolutional neural networks. *ACM Transactions on Graphics (TOG)*, 35(1):3, 2015. 1

[13] K. He, G. Gkioxari, P. Dollár, and R. Girshick. Mask r-cnn. In *ICCV*, 2017. 1

[14] K. He, X. Zhang, S. Ren, and J. Sun. Deep Residual Learning for Image Recognition. In *CVPR*, 2016. 1

[15] S. Hochreiter and J. Schmidhuber. Long short-term memory. *Neural computation*, 9(8):1735–1780, 1997. 5

[16] G. Huang, Z. Liu, L. van der Maaten, and K. Q. Weinberger. Densely connected convolutional networks. In *CVPR*, 2017. 1

[17] S. Ji, W. Xu, M. Yang, and K. Yu. 3d convolutional neural networks for human action recognition. *TPAMI*, 35(1):221–231, 2013. 1

[18] M. Kortgen, G. Park, M. Novotni, and R. Klein. 3d shape matching with 3d shape contexts. In *In the 7th Central European Seminar on Computer Graphics*, 2003. 3, 4

[19] A. Krizhevsky, I. Sutskever, and G. E. Hinton. Imagenet classification with deep convolutional neural networks. In *NIPS*, 2012. 1, 2

[20] Y. LeCun, B. Boser, J. S. Denker, D. Henderson, R. E. Howard, W. Hubbard, and L. D. Jackel. Backpropagation applied to handwritten zip code recognition. *Neural computation*, 1(4):541–551, 1989. 1, 2

[21] H. Ling and D. W. Jacobs. Shape classification using the inner-distance. *TPAMI*, 29(2):286–299, 2007. 2

[22] J. Long, E. Shelhamer, and T. Darrell. Fully convolutional networks for semantic segmentation. In *CVPR*, 2015. 1

[23] A. Payan and G. Montana. Predicting alzheimer's disease: a neuroimaging study with 3d convolutional neural networks. *arXiv preprint arXiv:1502.02506*, 2015. 1

[24] E. Perez, F. Strub, H. de Vries, V. Dumoulin, and A. Courville. Film: Visual reasoning with a general conditioning layer. In *AAAI*, 2018. 5

[25] C. R. Qi, L. Yi, H. Su, and L. J. Guibas. Pointnet++: Deep hierarchical feature learning on point sets in a metric space. In *NIPS*, 2017. 2, 5, 6, 7

[26] S. Ren, K. He, R. Girshick, and J. Sun. Faster r-cnn: Towards real-time object detection with region proposal networks. In *NIPS*, 2015. 1

[27] R. B. Rusu, N. Blodow, and M. Beetz. Fast point feature histograms (fpfh) for 3d registration. In *IEEE Robotics and Automation*, 2009. 1

[28] M. Savva, F. Yu, H. Su, M. Aono, B. Chen, D. Cohen-Or, W. Deng, H. Su, S. Bai, X. Bai, et al. Shrec16 track: large-scale 3d shape retrieval from shapenet core55. In *Eurographics Workshop on 3D Object Retrieval*, 2016. 1

[29] K. Simonyan and A. Zisserman. Very deep convolutional networks for large-scale image recognition. In *ICLR*, 2015. 1

[30] H. Su, S. Maji, E. Kalogerakis, and E. Learned-Miller. Multi-view convolutional neural networks for 3d shape recognition. In *ICCV*, 2015. 1

[31] C. Szegedy, W. Liu, Y. Jia, P. Sermanet, S. Reed, D. Anguelov, D. Erhan, V. Vanhoucke, and A. Rabinovich. Going deeper with convolutions. In *CVPR*, 2015. 1

[32] C. Szegedy, V. Vanhoucke, S. Ioffe, J. Shlens, and Z. Wojna. Rethinking the inception architecture for computer vision. In *CVPR*, 2016. 1

[33] D. Tran, L. Bourdev, R. Fergus, L. Torresani, and M. Paluri. Learning spatiotemporal features with 3d convolutional networks. In *ICCV*, 2015. 1

[34] D. Tran, H. Wang, L. Torresani, J. Ray, Y. LeCun, and M. Paluri. A closer look at spatiotemporal convolutions for action recognition. *arXiv preprint arXiv:1711.11248*, 2017. 1

[35] A. Vaswani, N. Shazeer, N. Parmar, J. Uszkoreit, L. Jones, A. N. Gomez, Ł. Kaiser, and I. Polosukhin. Attention is all you need. In *NIPS*, 2017. 2, 5, 6

[36] D. Z. Wang and I. Posner. Voting for voting in online point cloud object detection. In *Robotics: Science and Systems*, 2015. 1

[37] Z. Wu, R. Shou, Y. Wang, and X. Liu. Interactive shape co-segmentation via label propagation. *Computers & Graphics*, 38:248–254, 2014. 7

[38] Z. Wu, S. Song, A. Khosla, F. Yu, L. Zhang, X. Tang, and J. Xiao. 3d shapenets: A deep representation for volumetric shapes. In *CVPR*, 2015. 1, 2, 6

[39] S. Xie, R. Girshick, P. Dollár, Z. Tu, and K. He. Aggregated residual transformations for deep neural networks. In *CVPR*, 2017. 1

[40] S. Xie, C. Sun, J. Huang, Z. Tu, and K. Murphy. Rethinking spatiotemporal feature learning for video understanding. *arXiv preprint arXiv:1712.04851*, 2017. 1

[41] K. Xu, J. Ba, R. Kiros, K. Cho, A. Courville, R. Salakhudinov, R. Zemel, and Y. Bengio. Show, attend and tell: Neural image caption generation with visual attention. In *ICML*, 2015. 2

[42] L. Yi, V. G. Kim, D. Ceylan, I. Shen, M. Yan, H. Su, A. Lu, Q. Huang, A. Sheffer, L. Guibas, et al. A scalable active framework for region annotation in 3d shape collections. *ACM Transactions on Graphics (TOG)*, 35(6):210, 2016. 1, 2, 7

[43] B. Zoph and Q. V. Le. Neural architecture search with reinforcement learning. In *ICLR*, 2017. 1